JOURNAL OF COMPUTATIONAL PHYSICS 43, 1–15 (1981)

Numerical Solution of Hyperbolic Equations for Electron Drift in Strongly Non-Uniform Electric Fields

R. MORROW

Division of Applied Physics, CSIRO, Sydney, Australia 2070

Received September 25, 1980; revised May 22, 1981

A comparison is made of solutions of the continuity equations for the motion of electrons and ions in a strong electric field using the methods of Euler, Runge–Kutta, Lax–Wendroff, characteristics and the flux-corrected transport (FCT) algorithm "Phoenical LPE Shasta" developed by Boris and Book (*J. Comput. Phys.* **20** (1976), 397), with their flux limiter and with the new flux limiting algorithms developed by Zalesak (*J. Comput. Phys.* **31** (1979), 335). Results with and without ionization, and for uniform and non-uniform electric fields, are compared. Because ionization by electrons is strongly dependent on the electric field, considerable care needs to be taken to choose an optimum numerical scheme for non-uniform fields. For example, the calculation of the properties of corona discharges, or the cathode-fall of a glow discharge, requires fine spatial resolution. It is found that the Lax–Wendroff method and the method of characteristics give acceptable results; however, the Phoenical LPE Shasta algorithm with the flux limiting algorithm of Zalesak gives the best results, with the added advantage of suppressing spurious oscillations.

1. INTRODUCTION

Theoretical predictions of the properties of the corona discharge, the cathode fall of a glow discharge, the development of a spark, or the effects of space charge on plasma motion are difficult because of the strongly varying electric field as shown in the work of Davies *et al.* [1] and Morrow and Lowke [2]. In the present paper, we assume as a first approximation that electron drift velocities and ionization coefficients are those given by the equilibrium values for a uniform electric field, so that solutions can be obtained for the continuity equations. Even so, there are difficulties in obtaining time-dependent solutions, because of the fine spatial resolution that is required. Because of the additional requirement to integrate over long time intervals, it is essential to optimise the numerical integration scheme.

The continuity equation for the drift of electrons in an electric field is

$$\frac{\partial N}{\partial t} = S - \frac{\partial NW}{\partial x}, \tag{1}$$

where t is the time variable; x is the space variable; N is the electron number density; W is the electron drift velocity, which is a function of the electric field; and S is the

0021-9991/81/090001-15$02.00/0

source term, which may include the creation of electrons by ionization and the loss of electrons due to recombination and attachment. We wish to solve this equation for uniform and non-uniform electric fields.

Initially, we obtain results by neglecting the source term S in Eq. (1). The simplest method is to use Euler integration in time, with upwind differencing for the space variable [3]. Unfortunately, this method has strong numerical diffusion, which is proportional to the mesh size [4, 5]. However, Strang [6] has suggested that a fourth-order Runge–Kutta method in the time variable, and fourth-order central differences in the space variable, should be stable without diffusion. The practical use of high-order methods for hyperbolic systems has recently been advocated by Turkel [7]. This is attractive because of the high order of accuracy that is possible. Thus, a fourth-order Runge–Kutta method in time was coupled in turn with upwind differencing, simple central differencing, and fourth-order central differencing of the space variable.

Another approach is to use the Lax–Wendroff method as applied to shock waves [8]. Both the one- and two-step methods were evaluated.

The "leapfrog method" was also tested, but was found to be unstable, which was not unexpected [9].

The hybrid method of characteristics due to Hartree [10] was also applied. This method has been applied previously to this problem [1]; however, it is complex and cumbersome to code and is an iterative method which may not converge under some conditions.

Finally the flux corrected transport algorithms (FCT) of Boris and Book were applied [11, 12]. The particular transport algorithm eventually adopted was the "Phoenical LPE Shasta" algorithm, which is the most convenient algorithm for use with source terms and boundary conditions and is one of the most accurate methods [11, 12]. The original flux correction algorithm developed by Boris and Book was applied as well as the new flux correction algorithm proposed by Zalesak [13].

For all the non-FCT approaches the basic Courant–Friedrichs–Lewy condition must be obeyed for stability [9]; i.e., the time step Δt must be such that $\Delta t < \Delta x/W$, where Δx is the grid spacing [14]. The Shasta algorithm is restricted to $\Delta t < \Delta x/2W$ [12].

2. Methods of Solution

2.1. *The Source Term Neglected*

(a) *The Euler method.* With Euler integration it is necessary to use upwind differencing for stability.

(b) *The Runge–Kutta method.* A standard fourth-order Runge–Kutta integration was used for the time variable [15]. The space variable was treated in turn using upwind differences, simple central differences [15], and fourth-order central differences [16], as suggested by Strang [6]. The equation used for fourth-order central differences is

$$\frac{\partial U_i^j}{\partial x} = \frac{1}{12\Delta x}(U_{i-2}^j - 8U_{i-1}^j + 8U_{i+1}^j - U_{i+2}^j), \tag{2}$$

where $U_i^j = N_i^j W_i^j$, where j refers to the time step and i to the grid position.

(c) *The Lax–Wendroff method.* The standard two-step Lax–Wendroff method, [8–10, 14], was applied. See Section 2.2. The original one-step Lax–Wendroff method was also applied; in this case, it has the form

$$\begin{aligned} N_i^{j+1} &= N_i^j - \frac{1}{2}\frac{\Delta t}{\Delta x}[U_{i+1}^j - U_{i-1}^j] \\ &\quad + \frac{1}{4}\left(\frac{\Delta t}{\Delta x}\right)^2 [(W_{i+1}^j + W_i^j)(U_{i+1}^j - U_i^j) \\ &\quad - (W_i^j + W_{i-1}^j)(U_i^j - U_{i-1}^j)] \\ &= N_i^j + \Delta N_{LW}. \end{aligned} \tag{3}$$

(d) *The hybrid method of characteristics.* The method used is the hybrid method due to Hartree [10], Eq. (1), neglecting the source term S, being written

$$\frac{\partial N}{\partial t} + W\frac{\partial N}{\partial x} = -N\frac{\partial W}{\partial x} \tag{4a}$$

or

$$\frac{DN}{Dt} = -N\frac{\partial W}{\partial x}. \tag{4b}$$

Equation (4) is then integrated along characteristic lines for only one time step to give a solution at regular grid points. The method, which is of second order, is outlined succinctly by Ames [10], and some useful details are given by Davies and Evans [17]. Briefly the method involves an iterative determination of the best position of the characteristic line which terminates on a grid point at time $t + \Delta t$. This involves interpolation of density values between grid points at time t. The method is quite complex particularly once positive and negative ions are included as each species has separate characteristic lines, yet all must be solved simultaneously if the equations are coupled.

(e) *Phoenical LPE Shasta.* The method actually used in this case will be outlined in some detail, as Boris and Book give so many alternatives and there are some aspects which need to be defined in detail. The method takes the following steps [12]:

1. Compute a transported and diffused solution, $\bar{N}_i^{j+1}$, using an equation which in our notation is

$$\begin{aligned} \bar{N}_i^{j+1} &= N_i^j - \tfrac{1}{2}[\varepsilon_{i+1/2}(N_{i+1}^j + N_i^j) - \varepsilon_{i-1/2}(N_i^j + N_{i-1}^j)] \\ &\quad + [v_{i+1/2}(N_{i+1}^j - N_i^j) - v_{i-1/2}(N_i^j - N_{i-1}^j)], \end{aligned} \tag{5}$$

where $\varepsilon_{i+1/2} = W_{i+1/2}\,\Delta t/\Delta x$ and $W_{i+1/2}$ is the flow velocity half way between grid points i and $i+1$ calculated in this case by simple averaging. For the Phoenical LPE version of the Shasta algorithm,

$$v_{i+1/2} = \tfrac{1}{6} + \tfrac{1}{3}\varepsilon_{i+1/2}^2 .$$

2. Compute the raw antidiffusive fluxes which in our case for the Phoenical version are

$$\phi_{i+1/2} = \mu_{i+1/2}[\bar{N}_{i+1}^{j+1} - \bar{N}_i^{j+1} + (-N_{i+2}^j + 3N_{i+1}^j - 3N_i^j + N_{i-1}^j)/6], \tag{6}$$

where $\mu_{i+1/2} = (1 - \varepsilon_{i+1/2}^2)/6$.

3. Compute corrected antidiffusive fluxes, $\bar{\phi}$, using

$$\bar{\phi}_{i+1/2} = S \cdot \max\{0, \min[S \cdot (\bar{N}_{i+2}^{j+1} - \bar{N}_{i+1}^{j+1}), |\phi_{i+1/2}|, S \cdot (\bar{N}_i^{j+1} - \bar{N}_{i-1}^{j+1})]\}, \tag{7}$$

where $|S| = 1$ and $S \equiv \operatorname{sign}(\bar{N}_{i+1}^{j+1} - \bar{N}_i^{j+1})$.

4. Perform antidiffusion using

$$N_i^{j+1} = \bar{N}_i^{j+1} - \bar{\phi}_{i+1/2} + \bar{\phi}_{i-1/2}. \tag{8}$$

Thus N_i^{j+1} is the required solution at $t + \Delta t$.

The new algorithm for flux limiting developed by Zalesak [13], which is outlined succinctly in Section IV of his paper, was also applied. The method of avoiding "clipping" by predicting maxima and minima between grid points for use in flux limiting, outlined in Section V of Zalesak's paper, was also applied. In particular the flux constraint conditions described by Eq. (14) of Zalesak's paper were found to be quite important rather than cosmetic as suggested by Zalesak. In our notation the extra flux constraint is

$$\begin{aligned} \bar{\phi}_{i+1/2} = 0 \qquad & \text{if} \quad \phi_{i+1/2}(\bar{N}_{i+1}^{j+1} - \bar{N}_i^{j+1}) < 0 \\ & \text{and either} \quad \phi_{i+1/2}(\bar{N}_{i+2}^{j+1} - \bar{N}_{i+1}^{j+1}) < 0 \\ & \text{or} \quad \phi_{i+1/2}(\bar{N}_i^{j+1} - \bar{N}_{i-1}^{j+1}) < 0. \end{aligned} \tag{9}$$

2.2. *The Source Term Included*

For the Euler and Runge–Kutta methods, the source term is simply added to the convective term, such that

$$\Delta N = \Delta t \left(S_i^j - \frac{\partial N_i^j W_i^j}{\partial x} \right). \tag{10}$$

We proceed similarly for the method of characteristics.

For the Lax–Wendroff methods and the FCT method the source term must be introduced so that it is treated with second-order accuracy, as for the convective

term. For the one-step Lax–Wendroff method and the FCT method the increment in the electron density ΔN_c due to the convective term was calculated for a full time step. Then an auxiliary step was introduced by calculating the complete $\Delta N_{T_{1/2}}$ at half the time step, using the equation

$$\Delta N_{T_{1/2}} = \frac{\Delta t}{2}(S_i^j) + \tfrac{1}{2}\Delta N_c. \tag{11}$$

This allows auxiliry values for the source terms $S_i^{j+1/2}$ to be calculated. Then a full step was calculated, using the equation

$$\Delta N_T = \Delta t(S_i^{j+1/2}) + \Delta N_c. \tag{12}$$

Thus, the source term is effectively integrated using a second-order Runge–Kutta technique [15].

The source term was introduced to the two-step Lax–Wendroff scheme in a slightly different way, as follows.

Auxiliary step:

$$N_{i+1/2}^{j+1/2} = \frac{1}{2}(N_i^j + N_{i+1}^j) - \frac{\Delta t}{2\Delta x}(N_{i+1}^j W_{i+1}^j - N_i^j W_i^j) + \frac{\Delta t}{4}(S_i^j + S_{i+1}^j). \tag{13}$$

Main step:

$$N_i^{j+1} = N_i^j - \frac{\Delta t}{\Delta x}(N_{i+1/2}^{j+1/2} W_{i+1/2}^{j+1/2} - N_{i-1/2}^{j+1/2} W_{i-1/2}^{j+1/2}) + \frac{\Delta t}{2}(S_{i+1/2}^{j+1/2} + S_{i-1/2}^{j+1/2}). \tag{14}$$

In this treatment, the source term is effectively evaluated by the second-order Runge–Kutta method, but with the difference that in the averaging process the source term is influenced by neighbouring grid points, whereas in the one-step case it is not. As a consequence, there are slight differences in the results for strong ionization in a non-uniform field.

The form of the source term introduced in this case is

$$S = N\alpha\,|W|, \tag{15}$$

where α is the ionization coefficient [1]. However, in other cases, terms may be included to take account of the effects of attachment and recombination; this couples the equation to the equations for positive and negative ions.

3. Initial Conditions

All the methods are applied using the same basic conditions as those used by Davies *et al.* [1]; these are outlined below. The electron densities are kept below the level where space charge effects need to be included.

The electrons start near the cathode and move between two plane, parallel electrodes 3 cm apart. This space is represented by a grid of 101 points; hence $\Delta x = 0.03$ cm. The initial electron pulse is either triangular (Figs. 1 and 3) or square (Fig. 5).

The uniform electric field was -5.58 kV/cm [1]. The non-uniform electric field was taken, for convenience, to be linearly decreasing in amplitude, and for the square-wave calculation (Fig. 5) decreased from -11.16 to -0.11 kV/cm. With ionization (Figs. 6 and 7) the field amplitude had to be reduced to -6.7 kV/cm decreasing to -0.066 kV/cm.

The electron velocity was given by

$$|W| = 2.9 \times 10^5 \, E/p \text{ cm} \cdot \text{sec}^{-1} \tag{16}$$

and the ionization coefficient by

$$\alpha/p = 5.7 \exp(-260 \, p/E), \tag{17}$$

where p is pressure [1]. The time step was $\Delta t = 5 \times 10^{-10}$ sec. The Courant–Friedrichs–Lewy condition [9] requires that $\Delta t < \Delta x/W$, and this was maintained throughout the calculations for all the non-FCT methods. For the FCT methods the condition becomes $\Delta t < \Delta x/2w$ [12].

In all methods except the FCT methods the electron density N was maintained positive or zero, i.e.,

$$N \geqslant 0,$$

so that a calculated negative density was set equal to zero.

The Phoenical LPE Shasta method maintains positivity when the flux correction algorithms of Boris and Book [12] are used and the above measure is not required. However, when the new flux correction algorithm of Zalesak is applied the calculated densities do dip slightly below zero, thus as a countermeasure, in the spirit of the FCT method, the transported and diffused solution was used when the density became negative, guaranteeing positivity.

4. Results and Discussion

4.1. *Solutions Neglecting the Source Term and with a Uniform Electric Field*

For the results of this section, the standard triangular electron pulse near the cathode was used.

(a) *The Euler method with upwind differencing.* As predicted, the results show strong numerical diffusion, as shown in Figs. 1a and 2, where the initial electron pulse is modified unacceptably.

(b) *The Runge–Kutta method.* The introduction of Runge–Kutta integration in time with upwind differencing had no effect on the numerical diffusion, and the results were comparable with Fig. 1a.

When fourth-order central differences were used for the space variable, the results shown in Fig. 1b were obtained. These results show a small amount of dispersion, which removes the sharp corners, and very little dissipation. The position of the main peak coincides with the ideal position of the initial triangle displaced by a distance $D = tW$ along the x axis, as shown in Fig. 2. This ideal behaviour is marred by the appearance of the spurious smaller peaks behind the main pulse, seen more clearly in Fig. 2. As outlined by Roache [8], the spurious peaks are probably due to lack of dissipation in the equations. These small peaks grow rapidly when ionization is included, leading to unacceptable results.

With simple central differences, the results are stable and very similar to Fig. 1b, with the appearance of spurious peaks. However, there is some dissipation, and the peak heights slowly decay, as shown for the Lax–Wendroff method (Fig. 1c).

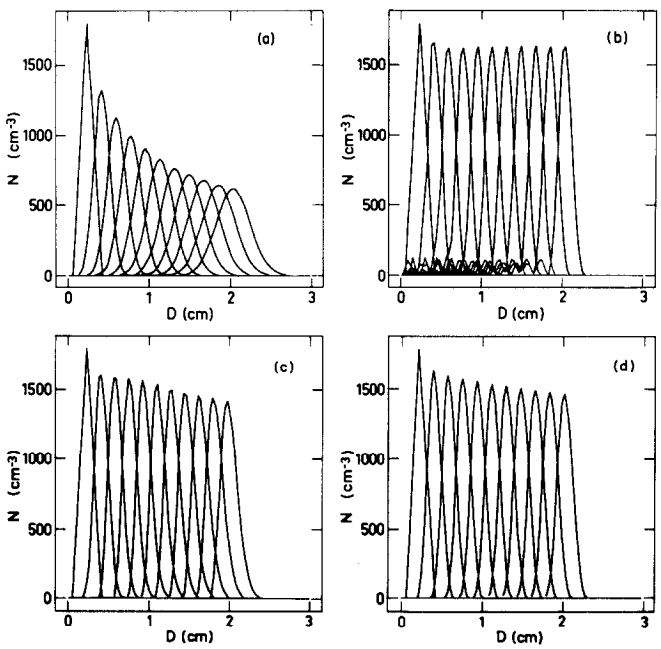

FIG. 1. Results of integration of Eq. (1), neglecting the source term, for a uniform electric field using various non-FCT algorithms. Calculations, with a triangular wave input at $t = 0$, were for 200 steps (100 nsec) with curves drawn every 20 steps (10 nsec). (a) Euler method with upwind differencing. (b) Fourth-order Runge–Kutta method with fourth-order central differences. (c) One- and two-step Lax–Wendroff methods. (d) Hybrid method of characteristics.

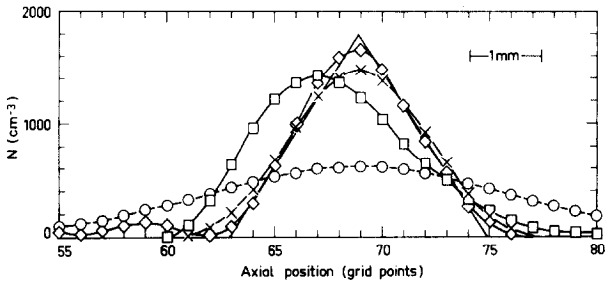

FIG. 2. Simultaneous comparison of results from Fig. 1 after 200 steps (100 nsec) with the initial triangular pulse of electrons displaced a distance $D = tW$ along the x axis, where $t = 100$ nsec. (——) Initial pulse. (○) Euler method. (◇) Runge–Kutta method. (□) Lax–Wendroff methods. (×) Hybrid method of characteristics.

(c) *The Lax–Wendroff method.* The one- and two-step Lax–Wendroff methods gave virtually indistinguishable results, as shown in Fig. 1c. In this case, there is a certain amount of dispersion and some dissipation. As shown in Fig. 2, the dispersion is slightly asymmetric, distorting the pulse so that it leans slightly backwards with a longer leading edge; this delays the pulse slightly compared with the ideal position of the initial triangle shown in Fig. 2.

(d) *The hybrid method of characteristics.* The results, shown in Fig. 1d, are very similar to the Lax–Wendroff results, with slightly less dispersion and dissipation. As shown in Fig. 2, the dispersion is symmetrical and the peak position is accurate.

(e) *Phoenical LPE Shasta.* Using the flux correction algorithm devised by Boris and Book, Eq. (7), the initial triangular wave is "clipped," as expected, and broadened as shown in Fig. 3a.

Using Zalesak's flux correction algorithm with flux also limited by the predicted maxima and minima between grid points but neglecting the flux contraint defined by Eqs. (9), the peaks are not clipped but small spurious peaks follow the main wave, as shown in Fig. 3b.

The result of using Zalesak's flux correction algorithm, including the conditions of Eqs. (9) but neglecting the flux limited by predicted maxima and minima, is shown in Fig. 3c. The spurious peaks disappear and the pulse shape is better preserved than for Fig. 3a.

Using Zalesak's full flux correction algorithm, including flux limited by predicted maxima and minima between grid points and the flux constraint defined by Eqs. (9), the results shown in Fig. 3d are obtained. There are no spurious peaks; thus, the spurious peaks are associated with the neglect of the flux constraint of Eqs. (9). The peak is as well preserved as that shown in Fig. 1b for the fourth-order Runge–Kutta with fourth-order central differences, without the associated spurious dispersive peaks. In fact when the curves of Fig. 3d are superimposed on those of Fig. 1b they almost exactly overlap.

In Fig. 4 the last curves, for $t = 100$ nsec, of Figs. 3a, c, and d are superimposed on

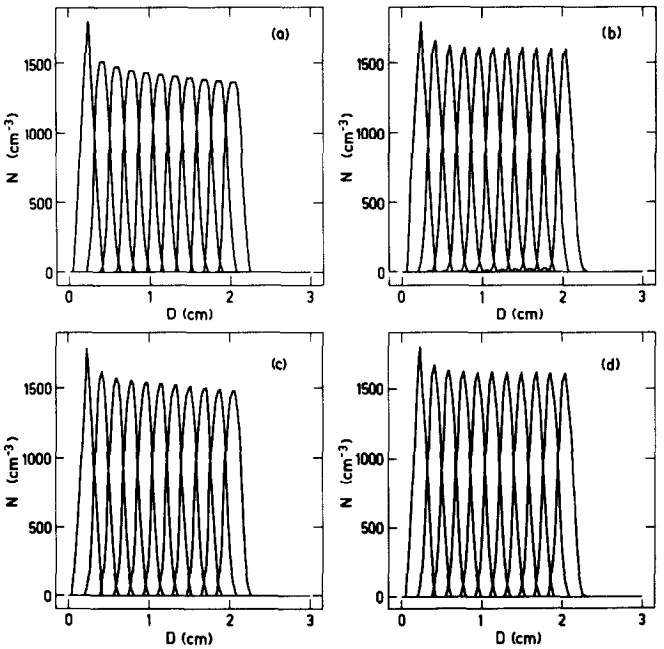

FIG. 3. Result of using the FCT algorithm phoenical LPE shasta to integrate Eq. (1), neglecting the source term, for a uniform field using various flux correction algorithms. Calculations with a triangular wave input were for 200 steps (100 nsec) with curves drawn every 20 steps (10 nsec). (a) Boris and Book's flux correction algorithm (Eq. (7)). (b) Zalesak's flux correction algorithm, including the use of predicted maxima and minima between grid points for flux correction but neglecting Eq. (9). (c) Zalesak's flux correction algorithm including Eq. (9) but neglecting the use of predicted maxima and minima between grid points. (d) Zalesak's flux correction algorithm including the use of predicted maxima and minima for flux correction and Eq. (9).

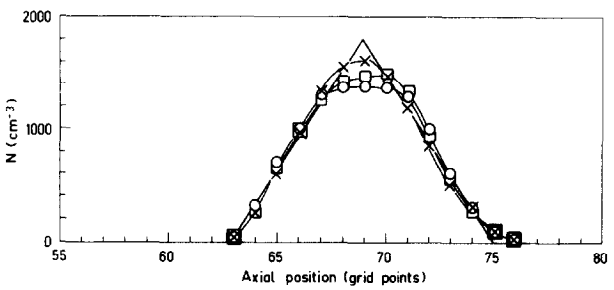

FIG. 4. Simultaneous comparison of results from Fig. 3 after 200 steps (100 nsec) with the initial triangular pulse of electrons displaced a distance $D = tw$ along the x axis, where $t = 100$ nsec. (——) Initial pulse. (○) Boris and Book's flux corrector. (□) Zalesak's full flux corrector less the peak preserver. (×) Zalesak's full flux corrector with peak preserver.

the curve for the initial triangle displaced a distance $D = tw$ along the x axis. The positions of all the peaks are very accurate, with the full Zalesak flux corrector giving the best results.

4.2. *Solutions Neglecting the Source Term and with a Non-Uniform Electric Field*

The use of an electric field of decreasing amplitude, as outlined in Section 3, resulted in all cases in the peak of the triangular wave increasing while the pulse width decreased. The same effect is illustrated more graphically using an initial square wave, as shown in Fig. 5 for various methods.

The physical implications of the results shown in Fig. 5 are interesting, since they indicate that a pulse of electrons will concentrate as it moves out of a high field region, due to the trailing electrons overtaking the leading electrons. The opposite happens when electrons move into an increasing electric field.

For the two step Lax–Wendroff method, Fig. 5a, dispersion causes a serious oscillation to develop on the leading edge; suppression of negative densities prevents similar oscillations from appearing on the trailing edge. The result of numerically integrating the electron density with respect to the space variable using the trapezoidal rule [15] for the initial and final distributions shows a net increase of 8% in the total electron density for Fig. 5a.

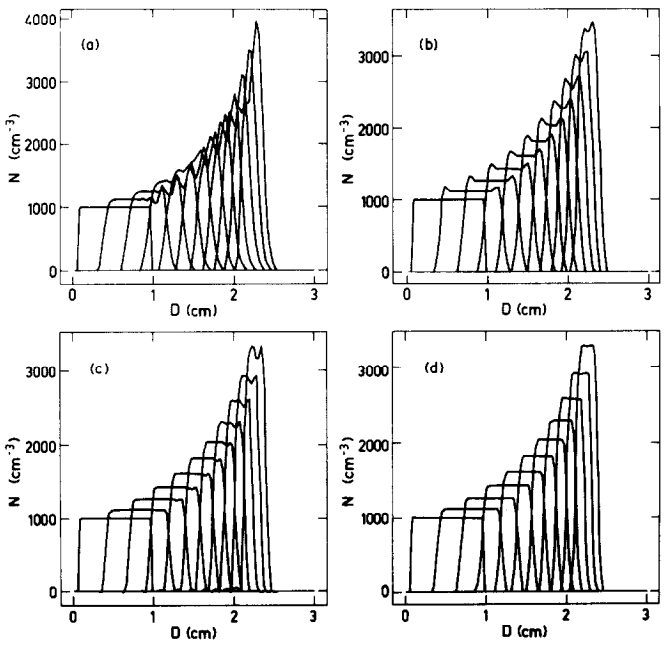

FIG. 5. Results of the integration of Eq. (1), neglecting the source term, for a linearly decreasing electric field using various algorithms. Calculations, with a square wave input, were for 200 steps (100 nsec) with curves drawn every 20 steps (10 nsec). (a) Two step Lax–Wendroff. ((b) Method of characteristics. (c) Phoenical LPE Shasta using the full Zalesak flux corrector but neglecting Eqs. (9). (d) Phoenical LPE Shasta using the full Zalesak flux corrector, including Eqs. (9).

The method of characteristics gives better results with symmetrical distortion of the leading and trailing edges as shown in Fig. 5b. Suppression of negative densities prevents negative distortions. The net density increased by 5% for Fig. 5b.

Figure 5c shows the results for the Phoenical LPE Shasta method using Zalesak's flux correction algorithm, including the peak preserver but neglecting Eqs. (9). Spurious peaks again appear at the trailing edge and a spurious trough near the leading edge is clearly due to neglecting the conditions of Eqs. (9), which are quite important in this case, rather than cosmetic as Zalesak suggests [13].

Including the extra flux conditions of Eqs. (9) removes these spurious peaks and troughs completely as shown in Fig. 5c, where the results are close to ideal. Integration of the electron density gives an increase of 1.4% in the first 30 nsec; then the integrated density does not change by more than 1 part in 10^8 from 30 to 100 nsec, a truly remarkable result since the distribution is transported and considerably modified from 30 to 100 nsec.

4.3. *Solutions Including the Source Term and a Uniform Electric Field*

The accuracy of the integration of the source term can be tested using a uniform electric field and a constant electron density throughout the space. The constant electron density constitutes a large square wave which moves along at velocity W while its top remains flat, so that $\partial NW/\partial x = 0$, and the electron density on the plateau increases as

$$N_t = N_0 \exp(\alpha t\,|\,W|), \tag{18}$$

where t is the elapsed time. With an initial electron density of 1000 cm^{-3}, the density calculated from Eq. (18) after 50 nsec was 1.055×10^6 cm^{-3} while all methods gave $n \approx 1.049 \times 10^6$ cm^{-3}, a difference of only 0.5%, which is quite acceptable.

4.4. *Solutions Including the Source Term and a Non-uniform Electric Field*

The results of introducing the source term with a non-uniform electric field are summarised for the five non-FCT methods in Fig. 6, and for the FCT methods in Fig. 7; both show the position at 60 nsec after 120 steps of the calculation. The results may be summarised as follows:

(a) *The Euler method.* Not only is there strong numerical diffusion, but with ionization in a non-uniform electric field this diffusion leads to more electrons being created upstream, thus inflating the trailing edge of the pulse and distorting it so that it is seriously delayed with respect to the other results, as shown in Fig. 6.

(b) *The Runge–Kutta method.* The small anomalous peaks shown in Fig. 2 are amplified in Fig. 6 to large proportions in the high field region behind the main pulse. However, the leading part of the pulse agrees very well with the hybrid method of characteristics.

(c) *The Lax–Wendroff methods.* The two Lax–Wendroff methods give results very close to those for the hybrid method of characteristics. The differences between

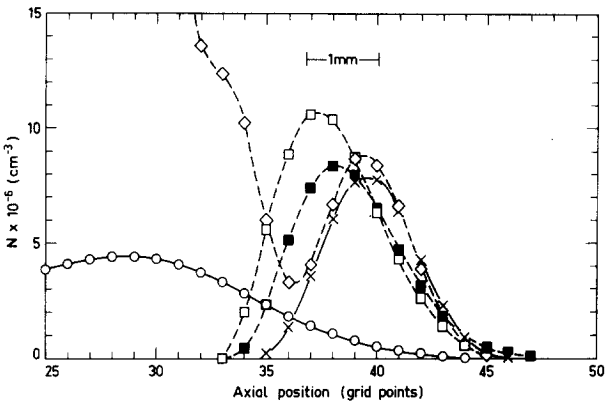

FIG. 6. Result of including an ionization source term in a non-uniform electric field for various non-FCT algorithms. Calculations were made with a triangular wave input and results are shown after 120 steps (60 nsec). (○) Euler method. (◇) Runge–Kutta method. (□) One-step Lax–Wendroff method. (■) Two-step Lax–Wendroff method. (×) Hybrid method of characteristics.

the two Lax–Wendroff methods are due to the slight differences in the treatment of the source term, discussed earlier. The two-step Lax–Wendroff method is closest to the method of characteristics. Both methods show some slight delay due to the slightly different dispersion of the Lax–Wendroff method compared with the method of characteristics noted earlier; see Fig. 2.

(d) *The hybrid method of characteristics.* The hybrid method of characteristics appears to be the most accurate non-FCT method. The results, relative to the other methods, shown in Fig. 6, are consistent with the results of Fig. 2.

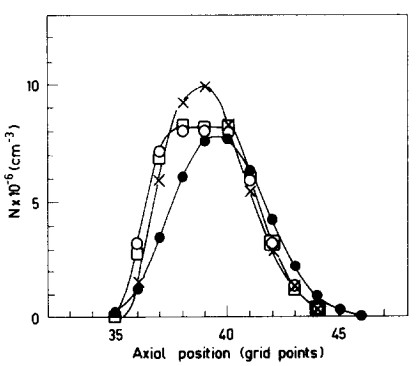

FIG. 7. Results of including an ionizing source term in a non-uniform electric field using the FCT algorithm Phoenical LPE Shasta and various flux correction algorithms. The results for the method of characteristics are shown for comparison. Calculations were made with a triangular wave input and are shown after 120 steps (60 nsec). (○) Boris and Book's flux corrector. (□) Zalesak's full flux corrector less peak preserver. (×) Zalesak's full flux corrector including the peak preserver. (●) Method of characteristics.

(e) *Phoenical LPE Shasta.* The use of the flux correction algorithms of Boris and Book or Zalesak without the peak preserver gives very similar results with a flat top, as shown in Fig. 7. The use of Zalesak's algorithm with the peak preserver gives a much better shaped pulse, with a slightly different position, and with an amplitude significantly larger than that for the method of characteristics, shown for comparison in Fig. 7. The differences between the two methods stem from the fact that the FCT method preserves the shape of the initial pulse more accurately and small differences in pulse shape lead to significant differences when a non-uniform electric field is applied together with a non-linear ionization coefficient, giving a non-linear source term.

4.5. *Computing Times*

In Table I a comparison is made of the central processor execution times for calculations using the different algorithms to obtain the results shown in Figs. 1 and 3. The computer used was the CSIRO Cyber 76 in Canberra. Note that these times are only relative and do not refer to the simple application of the algorithm since the programs, in all cases, include positive and negative ion calculations as well as ionization, attachment, recombination, and space charge effects, which have all been removed by setting suitable coefficients to zero, but which still contribute to the central processor time.

The Runge–Kutta method is the most complex method and therefore takes the longest time while the Euler method is the simplest and takes the shortest time. The method of characteristics takes the second longest time for the simple problem of Fig. 1; however, for the more complex problem of Fig. 6 more iterations are required and the time taken was 22 sec, while the time remains the same for the other methods.

The two Lax–Wendroff methods take similar times, while the Boris and Book algorithm, Phoenical LPE Shasta, takes only 10% more time, and the full Zalesak algorithms only 20% more time.

TABLE I

Comparison of Central Processor (CP) Execution Times

Method	CP time (sec)
Euler with upwind differencing	7.3
Runge–Kutta	17.9
Lax–Wendroff, one step	9.6
Lax–Wendroff, two step	9.9
Method of characteristics	14.2[a]
Phoenical LPE Shasta (Boris and Book)	10.9
Phoenical LPE Shasta (full Zalesak treatment)	12.3

[a] Note that the method of characteristics is an iterative process and takes longer to converge for some problems, for example, with the ionization calculation of Fig. 6 the CP time was 22.0 sec.

5. Conclusions

The Euler method with upwind differencing is unacceptable due to numerical diffusion and the fourth-order Runge–Kutta method with fourth-order central differences is unacceptable due to the appearance of spurious peaks.

The two Lax–Wendroff methods and the method of characteristics all give satisfactory results in most cases, particularly for the difficult case of a non-uniform field with a finite source term. Both methods exhibit distortions when propagating sharp discontinuities such as a square wave. The method of characteristics is the most accurate non-FCT method tested.

The FCT method "Phoenical LPE Shasta" using the full flux correction algorithm of Zalesak, including the peak preserving method, gave the best results, which in all cases used were close to ideal. In particular it is not clear from the literature how well the FCT method performs in non-uniform electric and velocity fields of interest for electric discharges. The performance of the FCT method in non-uniform electric fields with and without a finite source term was excellent, giving very good results compared with other quite different methods, which gives considerable confidence in the method, in this area where analytic checks are not available. The FCT method does not use significantly greater computer time than the Lax–Wendroff method and uses less time than its closest rival, the method of characteristics.

Acknowledgments

I would like to acknowledge much encouragement from, and many helpful discussions with, Dr. John J. Lowke of this Laboratory. I must thank Dr. Clive Fletcher for many helpful discussions. I would also like to thank Dr. J. Atkinson and Dr. J. Knight for their help.

References

1. A. J. Davies, C. S. Davies, and C. J. Evans, *Proc. Inst. Electr. Engrs.* **118** (1971), 816.
2. R. Morrow and J. J. Lowke, *J. Phys. D.*, in press.
3. C. K. Chu, *in* "Advances in Applied Mechanics" (Chia-Shun Yih, Ed.), p. 286, Academic Press, New York, 1978.
4. A. L. Ward, *J. Appl. Phys.* **36** (1965), 1291.
5. L. E. Kline, *J. Appl. Phys.* **45** (1974), 2046.
6. G. Strang, *Numer. Math.* **6** (1964), pp. 37–46.
7. E. Turkel, "On the Practical Use of High Order Methods for Hyperbolic Systems," ICASE Report No. 78-19, Institute for Computer Applications in Science and Engineering, NASA Langley Research Centre, Hampton, Va., Nov. 16, 1978.
8. P. J. Roache, "Computational Fluid Dynamics," Hermosa, Albuquerque, 1972.
9. D. Potter, "Computational Physics," Wiley, Chichester/New York, 1977.
10. W. F. Ames, "Numerical Methods for Partial Differential Equations," Academic Press, New York, 1977.
11. J. P. Boris and D. L. Book, *J. Comput. Phys.* **20** (1976), 397–431.

12. J. P. BORIS AND D. L. BOOK, *in* "Methods in Computational Physics" (John Killeen, Ed.), pp. 85–130, Academic Press, New York, 1976.
13. S. T. ZALESAK, *J. Comput. Phys.* **31** (1979), 335–362.
14. R. D. RICHMYER AND K. W. MORTON, "Difference Methods for Initial-Value Problems," Interscience, New York/London, 1967.
15. M. ABRAMOWITZ AND I. A. STEGUN, "Handbook of Mathematical Functions," Dover, New York, 1965.
16. C. R. WYLIE, "Advanced Engineering Mathematics," McGraw–Hill, New York, 1960.
17. A. J. DAVIES AND C. J. EVANS, "Theory of Ionization Growth in Gases under Pulsed and Static Fields," Report to CERN European Organization for Nuclear Research, Geneva, 1973.